Research Square

Preprints are preliminary reports that have not undergone peer review.
They should not be considered conclusive, used to inform clinical practice,
or referenced by the media as validated information.

Structure and Sequence Regulated Biodegradable and Chemically Recyclable Adhesives

Zhen Zhang

zhenzhang@scut.edu.cn

South China University of Technology https://orcid.org/0000-0002-1188-5209

Beiwen Mo

South China University of Technology

Lin Zhu

South China University of Technology

Ze Xiao

South China University of Technology

Bixuan Wang

South China University of Technology

Ethan Quinn

California Institute of Technology

Yan Cao

South China University of Technology

Article

Keywords:

Posted Date: July 10th, 2026

DOI: https://doi.org/10.21203/rs.3.rs-10194242/v1

License: This work is licensed under a Creative Commons Attribution 4.0 International License.
Read Full License

Additional Declarations: There is **NO** Competing Interest.

Structure and Sequence Regulated Biodegradable and Chemically Recyclable Adhesives

Beiwen Mo [1†], Lin Zhu [1†], Ze Xiao[1], Bixuan Wang[1], Ethan C. Quinn[2], Yan Cao[1,3], and Zhen Zhang[1,3*]

[1] Advanced Institute for Soft Matter Science and Technology (AISMST), School of Emergent Soft Matter, State Key Laboratory of Pulp and Paper Engineering, South China University of Technology, Guangzhou 510640, China

[2] Division of Chemistry and Chemical Engineering, California Institute of Technology, Pasadena, California 91125, United States

[3] Guangdong Provincial Key Laboratory of Functional and Intelligent Hybrid Materials and Devices, Guangdong Basic Research Center of Excellence for Energy and Information Polymer Materials
South China University of Technology, Guangzhou 510640, China

[†]These authors contributed equally to this work

*Correspondence to: zhenzhang@scut.edu.cn (Z. Zhang)

Abstract: Polymeric adhesives play a pivotal role in modern society; however, most commercial formulations are petroleum-derived and non-degradable, posing significant environmental concerns. To address sustainability requirements, a broad range of synthetic polymers have been explored over the past decades. Nevertheless, rational strategies to impart robust adhesive properties to typical sustainable polymers remain elusive due to the complex interplay of factors governing adhesion, particularly those associated with polymer backbone microstructure and the nature of functional groups. Moreover, sustainable adhesives should be chemically recyclable when recovery is feasible and biodegradable as adhesives are frequently leaked into the environment. Herein, we report a series of biodegradable and chemically recyclable copolyester adhesives derived from δ-valerolactone and hydroxyl-functionalized derivatives. By rationally introducing stereodefects into polymer backbones, incorporating hydrogen-bonding moieties into the side chains, and controlling segment sequence distribution, the resulting materials exhibit widely tunable adhesion strengths ranging from 2.3 to 12.3 MPa across diverse substrates while maintaining favorable thermomechanical properties and chemical recyclability.

Introduction

Polymeric adhesives, as a class of essential functional materials that can efficiently and reliably bond various substrates, play a pivotal role in modern society, underpinning diverse sectors ranging from daily life and industrial production to constructions and healthcare.[1-4] At present, commonly used adhesives are predominantly derived from non-renewable petroleum resource and are not biodegradable, thus raising growing concerns regarding their environmental footprint.[5-7] Furthermore, the frequently employed volatile organic solvent and/or hazardous tackifier additives in traditional adhesives pose extra safety issue during applications, particularly in the fields of medical

supply and food-contact packaging.[8] These issues highlight an urgent need for sustainable alternatives that are ideally bio-derived, biocompatible, and biodegradable. To meet these sustainability criteria, a wide range of natural and synthetic polymers have been explored and developed over the past decades.[9-13] However, rationally imparting adhesive properties to these materials remains challenging due to the complex interplay of adhesion-governing factors, particularly those arising from polymer backbone microstructures and functional groups.

Stereomicrostructural regulation of polymer backbone is an effective pathway to tune the thermomechanical, viscoelastic, and even adhesive properties of polymeric materials. For example, increasing the tacticity of polylactic acid (PLA) gradually transforms the polymer from an amorphous to a semicrystalline state, accompanied by a substantial increase in its glass transition temperature from ~20 °C to ~67 °C.[14] Intentionally introducing stereodefects into the polymer backbone of stereo-regular poly(3-hydroxybutyrate) (P3HB) effectively decreased the domain size of crystalline moiety, leading to substantially enhanced mechanical toughness from 0.9 to 96 MJ/m^3 and dramatically improved optical transmittance value to 92% while maintaining its biodegradability, crystallinity, and barrier properties.[15] More interestingly, in contrast to isotactic and iso-rich P3HB, which exhibit negligible adhesive behavior, the stereoselectively synthesized syndio-rich P3HB displays strong adhesion across various substrates, with strengths up to 10 MPa that surpasses those of many widely used commercial adhesives.[16]

Physical interaction from specific functional groups, such as hydrogen-bonding and ionic interactions, is critical in the design of strong adhesives, as demonstrated in the polymeric systems of poly(α-lipoic acid)[17], thermoplastic elastomers[18], crosslinked epoxy resin[19], or uncondensed lignins[20]. The physical interaction plays important roles in several aspects, including interfacial adhesion at the surfaces, cohesive strength within the adhesives, and energy dissipation upon external loading. Specifically, the physical interaction ensures good interfacial contact, allowing the adhesive to conform to microscopic surface roughness of the substrates and anchor effectively. Besides, the dynamic nature of physical interaction, capable of reversible breaking and reformation, enables effective energy dissipation and suppresses crack propagation,[21] thereby enhancing material toughness, improving adhesion performance, and imparting reprocessability.

Polymer chain sequence, namely the consecutive ordering of the repeating units within a polymer backbone, is another important and intensively studied factor to modulate material properties and the adhesive behavior.[22-25] One well-known and commonly adopted strategy is the construction of soft and hard blocks along the polymer backbone, where the two individual segments play complementary and synergistic roles that give rise to their unique combination of viscoelasticity and mechanical strength.[26-28] The specific arrangement of polymeric blocks also found useful in the design of adhesives. In a recent study, Miyake and coworkers demonstrated that tuning the arrangement and content of crystalline hard blocks, amorphous soft blocks, and ester groups in a series of polyolefin-like multiblock copolymers can effectively improve their adhesive performance, offering an adhesion

strength of up to 6.8 MPa , approximately 80% higher than that of the widely used poly(ethylene-co-vinyl acetate) (EVA) hot-melt adhesive.[29] The advantage of bocky structure is that the high mobility of soft block allows absorption and dissipation of mechanical energy and provide intimate contact with other substrates, while the crystalline blocks act as reversible junctions to reinforce the material, resist deformation, and anchor soft chains.

In the development of biodegradable adhesives, it is more practical to focus on well-established biodegradable polymers. Most newly synthesized polymers have not co-evolved with biological systems and therefore lack corresponding enzymes capable of recognizing and cleaving their backbones under natural conditions, resulting in significantly reduced or even completely disappeared biodegradability.[30] Herein, we demonstrated the development of high-performance biodegradable adhesives based on poly(δ-valerolactone) (PVL), a chemically well-defined and biologically friendly polyester possessing universal degradability and great biocompatibility,[31-33] by leveraging stereomicrostructure manipulation, physical interactions, and chain-sequence regulation (Figure 1). Through rationalized strategies, namely installing stereodefects on PVL mainchain, introducing hydrogen-bonding interactions into the sidechain, and controlling the segment sequence, the thermomechanical and viscoelastic properties as well as the adhesive behavior of the resulting polymer were substantially reshaped, leading to significantly enhanced and widely tunable adhesion performance from 2.3 MPa to 12.3 MPa across various substrates while maintaining the great thermomechanical properties and chemical recyclability.

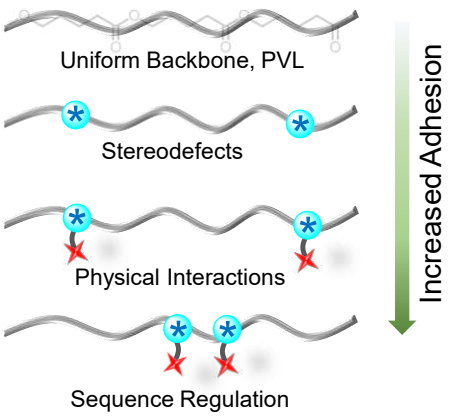


Figure 1. The design principle of PVL copolymer adhesives by leveraging stereodefects, physical interactions, and sequence regulation.

Results and Discussion

The cyclic monomers bearing designer stereogenic centers and diverse substituents, including silyl protected hydroxyl and alkyl groups (M_1 and M_2, Figure 2), were synthesized via one-step thiol-Michael addition reaction between biomass-derived 5,6-dihydro-2H-pyran-2-one and corresponding thiol compounds. The reactions proceeded in high yields (>90%) and afforded products with high purity, as confirmed by the ^{1}H NMR spectra (Figures S1-S3). Non-stereoselective ring-opening copolymerization (ROCOP) of δ-valerolactone (δ-VL) with

racemic M_1 was employed to introduce stereodefects into the PVL backbone. Subsequent deprotection of the dimethyl(2-methylprop-2-yl)silyl groups afforded polyesters bearing hydroxyl side chains, denoted as *r*-PVL(OH)$_x$, where *r* and x represent the randomness of comonomer sequence and the molar incorporation ratio of hydroxyl groups, respectively (Figure 2). La[N(SiMe$_3$)$_2$]$_3$ was selected as the ROCOP catalyst due to its high reactivity toward δ-VL and achiral nature leading to non-stereoselective polymerization.[34, 35] This system enabled precise control over molar mass while introducing stereoirregularity along the polymer backbone, thereby disrupting the crystalline domains of PVL and enhancing the viscoelastic character of the resulting polymer. The molar mass was deliberately controlled to be similar across samples, within the range of 30-42 kDa, to enable meaningful properties comparison among different polymers and target optimal adhesion performance (Figure S9). Successful copolymerization was confirmed by ^{1}H NMR spectroscopy showing increased resonance intensity from the functional side groups (Figures 3A and 3B) as well as by diffusion-ordered spectroscopy (DOSY), where identical diffusion coefficients for all polymer resonances indicated incorporation into a single macromolecular species (Figure 3C). The copolymerization kinetics were monitored by measuring the monomer conversion as a function of time (Figure 3D). Both δ-VL and M_1 were consumed concurrently, reaching maximum conversion within 5 min. This behavior indicates a random distribution of comonomer units along the polymer backbone under the one-pot ROCOP conditions.

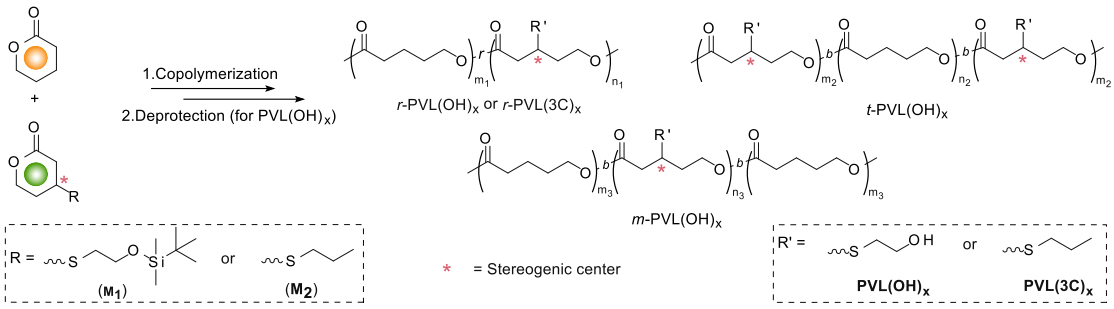


Figure 2. Synthetic route towards PVL(OH)$_x$ and PVL(3C)$_x$.

Table 1. Selected ROP results of PVL, PVL(OH)$_x$ and PVL(3C)$_x$.[a]

Run	[M]/[Cat.]/[I]	Time (h)	δ-VL/M_1	Conv.[b] (δ-VL%)	Conv.[b] (M_1 or M_2%)	Incorp.[b] (M_1 or M_2%)	M_n[c] (kg/mol^{-1})	$Đ$[d]	Sample
1	550/1/3	3	550/-	-[e]	-[e]	-[e]	35	1.7	PVL
2	550/1/3	1	542/8	98	95	1.5	32	1.6	*r*-PVL(OH)$_{1.5}$
3	550/1/3	1	539/11	99	94	2.2	34	1.7	*r*-PVL(OH)$_{2.2}$
4	550/1/3	1	524/28	98	91	4.9	34	1.7	*r*-PVL(OH)$_{4.9}$
5	550/1/3	1	495/55	98	88	9.0	30	1.5	*r*-PVL(OH)$_{9.0}$
6	600/1/3	1	510/90	98	88	10.0	39	1.4	*r*-PVL(OH)$_{10.0}$
7	900/1/3	2	882/18 (M_2)	97	91	1.7 (M_2)	42	2.0	*r*-PVL(3C)$_{1.7}$
8[f]	300/1/1.5	3	270/30	93	83	5.0	34	1.4	*t*-PVL(OH)$_{5.0}$

9[g]	200/1/1.5	3	188/12	99	78	5.3	38	1.6	*m*-PVL(OH)$_{5.3}$

[a] Polymerization conditions: La[N(SiMe$_3$)$_2$]$_3$ as catalyst, benzyl alcohol as initiator, [M] = 3M in toluene, room temperature (~25 °C); [b] Monomer conversions and incorporations of the copolymers were measured by ^{1}H NMR spectra; [c] Number-average molecular weight was determined by gel permeation chromatography (GPC) at rt in THF; [d] Dispersity index ($Đ$ = M_w/M_n); [e] Not determined; [f] 1,4-benzenedimethanol was used as initiator, and the hydroxyl groups are distributed at the chain terminus; [g] 1,4-benzenedimethanol was used as initiator, and the hydroxyl groups are distributed in the middle of the chain.

The molar incorporation of stereodefects and hydroxyl groups can be precisely tuned from 1.5% to 10% by varying the feeding ratio of δ-VL to M_1, and the resulting *r*-PVL(OH)$_x$ polymers exhibit comparable molar masses and narrow dispersities ($Đ$ = 1.4–1.7; Table 1, runs 1–6). As a control system involving only stereodefect incorporation and lacking hydrogen-bonding side chains, M_2 bearing a propyl side chain was copolymerized with δ-VL to afford *r*-PVL(3C)$_x$ (3C denotes the propyl group; Table 1, run 7), where the length of side chains was purposely chosen to be comparable to that of the hydroxyl-containing substituents. To regulate the repeating-unit sequence, that is, the placement of hydroxyl groups at the chain termini or in the middle of the chain, sequential copolymerization was conducted using 1,4-benzenedimethanol diinitiator. Specifically, δ-VL was firstly polymerized to generate a PVL block, followed by polymerization of M_1, and the subsequent deprotection yielded the formation of *t*-PVL(OH)$_x$ (*t* denotes hydroxyl groups located at the chain termini; Table 1, run 8). Conversely, the sequential polymerization of M_1 followed by δ-VL led to *m*-PVL(OH)$_x$ (*m* denotes hydroxyl groups located in the middle of the chain; Table 1, run 9).

To evaluate the impact of stereodefects and functional side chains on thermal transition behaviors, differential scanning calorimetry (DSC) was performed on the synthesized polymers (Figure 3E). Compared to PVL, *r*-PVL(3C)$_{1.7}$, containing 1.7 mol% of stereodefects, exhibited a reduced melting transition temperature (T_m) from 57 °C to 51 °C, along with decreased heat of fusion (ΔH_f) value from 67.5 to 53.1 J g^{-1} and crystallinity (X_c) from 37% to 29% (Figure 3F), indicating effective disruption of crystalline domains by the incorporated stereodefects. Switching the propyl side chain with hydroxyl groups led to a slight increase in T_m by 1 °C, an increase in ΔH_f value to 57.8 J g^{-1}, and a higher X_c of 32%, which can be attributed to the modest promotion of crystallization by hydrogen-bonding interactions.[36, 37] However, further increasing the hydroxyl content from 1.5 mol% to 4.9 mol% and ultimately to 10 mol% resulted in a progressive decrease in T_m, ΔH_f, and X_c to approximately 40 °C, 40.8 J g^{-1}, and 22%, respectively. This trend suggests that, at higher incorporation levels, the disruptive effect of stereodefects outweighs the crystallization-enhancing contribution of hydrogen-bonding interactions. The suppressive effect of stereodefects on crystalline domains was further corroborated by polarized light optical microscopy (PLOM), as shown in Figure 3G. Compared to PVL, which exhibits large, well-defined spherulites due to its high backbone regularity, *r*-PVL(3C)$_{1.7}$ and *r*-PVL(OH)$_{1.5}$, containing a low level of stereodefects (1–2 mol% relative to repeating units), displayed significantly reduced spherulite sizes. This reduction is attributed to enhanced nucleation and disruption of crystallizable sequences by randomly distributed

stereodefects along the PVL backbone. Thermogravimetric analysis (TGA) indicates that both PVL and its derivatives possess practical thermal stability, with decomposition temperatures (T_d, defined as the temperature at 5% weight loss) exceeding 250 °C, providing a broad processing window of over 200 °C. Notably, *r*-PVL(OH)$_{1.5}$, containing 1.5 mol% hydroxyl groups, exhibits an elevated T_d of 325 °C, which is 49 °C higher than that of PVL (T_d = 276 °C). In contrast, *r*-PVL(3C)$_{1.7}$, bearing 1.7 mol% propyl groups, shows a lower T_d of 258 °C (Figure 3H), highlighting the beneficial role of hydrogen-bonding interactions in enhancing thermal stability.[38-40]

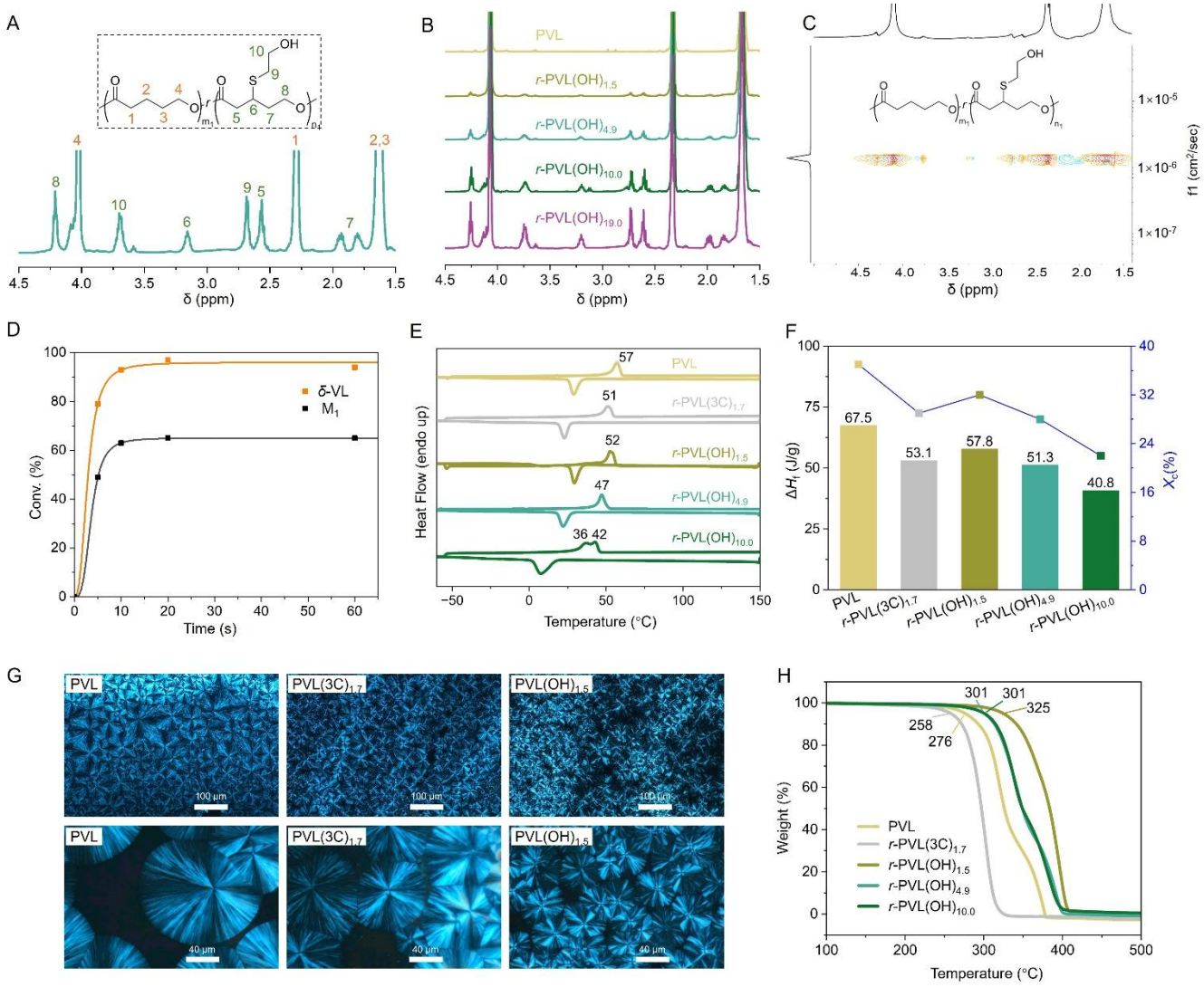


Figure 3. (A) ^{1}H NMR spectrum of *r*-PVL(OH)$_{19.0}$. (B) ^{1}H NMR spectra overlay of PVL and *r*-PVL(OH)$_{1.5\text{-}19.0}$. (C) DOSY spectrum of *r*-PVL(OH)$_{4.9}$. (D) Plots of monomer conversions over time in the copolymerization of δ-VL and M_1 at a ratio of 19:1. (E) DSC traces of PVL, *r*-PVL(3C)$_{1.7}$, and *r*-PVL(OH)$_{1.5\text{-}10.0}$. Data collected from the 1st cooling and 2nd heating scans with a scan rate of 10 °C min^{-1}. (F) ΔH_f and X_c values of PVL, *r*-PVL(3C)$_{1.7}$, and *r*-PVL(OH)$_{1.5\text{-}10.0}$. X_c is calculated based on the ΔH_m^o value of 100% crystalline polymer, 18.2 kJ/mol.[41] (G) PLOM micrograph of PVL, *r*-PVL(3C)$_{1.7}$, and *r*-PVL(OH)$_{1.5}$. (H) TGA curves of PVL, *r*-PVL(3C)$_{1.7}$, and *r*-PVL(OH)$_{1.5\text{-}10.0}$.

The mechanical properties of polymers play a critical role in adhesive performance, influencing surface wetting, energy dissipation, and stress redistribution. Accordingly, the synthesized polymers were evaluated by uniaxial tensile testing, and the results are shown in Figures 4A and 4B. PVL was found to be a relatively tough polymer possessing a Young's modulus (E) of 355 MPa, yield stress (σ_y) of 11.6 MPa, and elongation at break (ε_B) of 606%

(Table S1). Consistent with the reduced crystallinity induced by stereodefect incorporation, *r*-PVL(3C)$_{1.7}$ displays a decreased E to 192 MPa, lower σ_y of 7.4 MPa, yet enhanced ε_B of 945% and increased toughness (U_T) by 61% (Table S2). With both stereodefects and hydrogen-bonding interactions incorporated, *r*-PVL(OH)$_{1.5}$ exhibited further improved ε_B of 971%, higher σ_y of 13.3 MPa, and a moderate E of 270 MPa (Table S3). Increasing the hydrogen-bond content to 4.9 mol% results in reduced modulus (E = 209 MPa) while maintaining high extensibility (ε_B = 944%) and stress (σ_y = 9.7 MPa; Table S4). Notably, a combination of high toughness and reduced modulus is generally advantageous for adhesive performance.[42, 43] It is worth noting that the specimen from *r*-PVL(OH)$_{10.0}$ was too mechanically weak to undergo tensile testing, indicating that excessive stereodefect incorporation overwhelms the reinforcing effect of hydrogen-bonding interactions. As a result, *r*-PVL(3C)$_{1.7}$, *r*-PVL(OH)$_{1.5}$, and *r*-PVL(OH)$_{4.9}$, with a suitable amount of stereodefects and/or hydrogen-bonding interactions, all exhibit high mechanical toughness (U_T >97 MJ m^{-3}) and adhesion-favorable low moduli (Figure 4B).

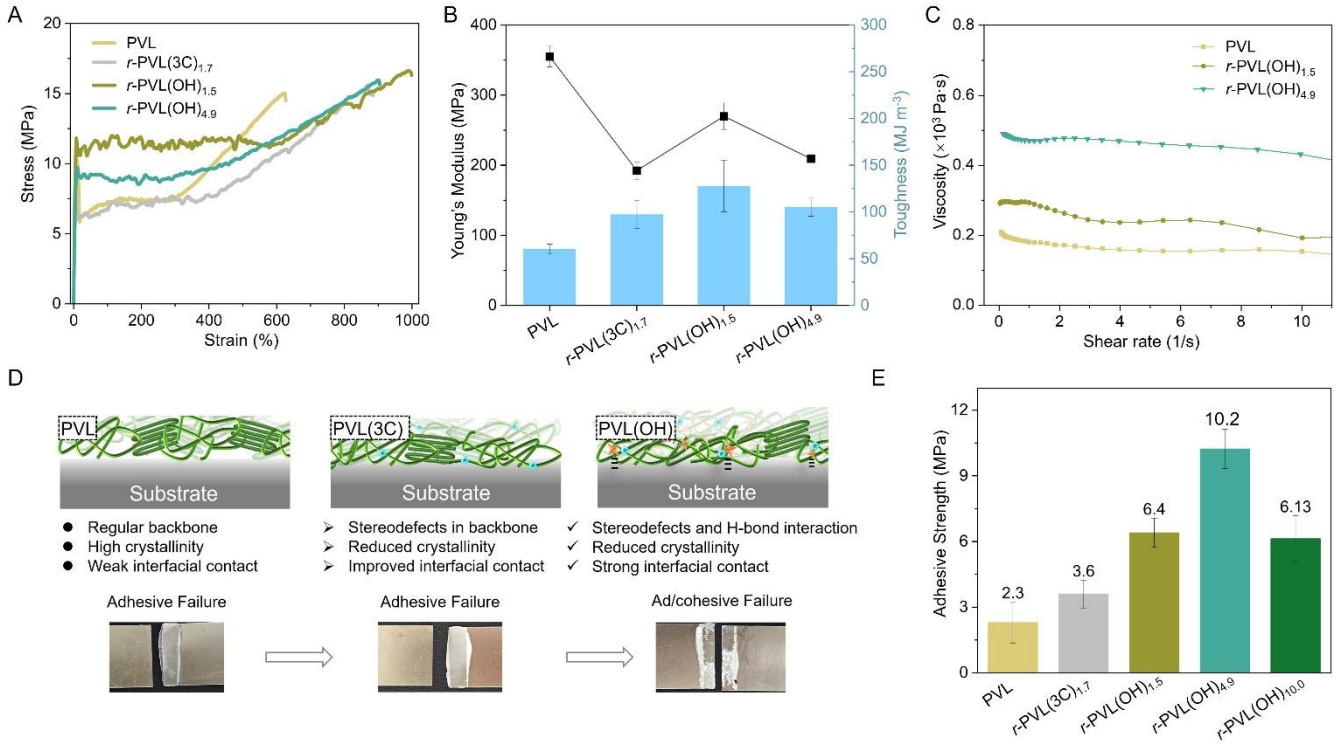


Figure 4. (A) Stress-strain curves of PVL, *r*-PVL(3C)$_{1.7}$, and *r*-PVL(OH)$_{1.5 \text{ and } 4.9}$. (B) Young's modulus and toughness of PVL, *r*-PVL(3C)$_{1.7}$, and *r*-PVL(OH)$_{1.5 \text{ and } 4.9}$. (C) Shear viscosity over shear rate of PVL and *r*-PVL(OH)$_{1.5 \text{ and } 4.9}$ in melt (65 °C). (D) Illustration of the adhesion formation at the interface of polymer and substrates. The bottom pictures show the failure modes of the specimens during lap-shear tests. (E) Adhesion strength of PVL, *r*-PVL(3C)$_{1.7}$, and *r*-PVL(OH)$_{1.5\text{-}10.0}$ on stainless steel. Error bars represent a standard deviation of three specimens.

The inter- and intramolecular strengthening effects from hydrogen-bonding interactions were further evidenced by melt viscosity measurements for polymers with comparable molar masses (32-35 kDa). As shown in Figure 4C, the melt viscosity increases progressively from ~200 to ~500 Pa·s with increasing hydrogen-bond content, indicating stronger inter- and intramolecular interactions. Importantly, the combination of low modulus, high toughness, and dynamic hydrogen-bonding interactions is expected to facilitate efficient surface wetting, energy dissipation, and interfacial anchoring during adhesion. These synergistic effects enhance both cohesive strength

within the polymer and adhesive interactions with substrates as illustrated in Figure 4D, which was further demonstrated in subsequent adhesion studies.

The adhesion performance of the designed polymers was systematically evaluated using lap-shear tests. In these measurements, the polymer was placed between two substrates to form a bonded joint via thermal melting, followed by solidification upon cooling. The resulting specimens were subjected to oppositely directed forces to simulate shear stresses commonly encountered under service conditions, and the maximum stress sustained prior to failure was recorded. The lap-shear adhesion strength was calculated by dividing the maximum failure force by the overlap area of the bonded substrates. As shown in Figure 4E, PVL displays a relatively low adhesion strength of 2.3 MPa. Upon incorporation of stereodefects, *r*-PVL(3C)$_{1.7}$ exhibits an improved adhesion of 3.6 MPa, which can be attributed to its reduced modulus and consequently enhanced interfacial contact. Intriguingly, with stereodefects and hydrogen-bonding interactions simultaneously incorporated, *r*-PVL(OH)$_{1.5}$ shows significantly improved adhesion strength to 6.4 MPa. Further increasing the hydrogen-bond content to 4.9% elevates the adhesion strength to values exceeding 10 MPa, a level rarely achieved for biodegradable polyester-based materials and approaching strengths of structural adhesives. However, excessive incorporation of stereodefects and hydrogen bonds, as in *r*-PVL(OH)$_{10}$, results in a reduced adhesion strength of 6.1 MPa. This decline is attributed to severely disrupted crystalline domains and diminished cohesive strength, as evidenced by its low ΔH_f value and poor mechanical performance. From PVL to *r*-PVL(3C)$_{1.7}$ and further to *r*-PVL(OH)$_{1.5\text{-}10.0}$, the failure mode of the lap-shear specimens progressively transitions from adhesive to cohesive as shown in Figure 4D, highlighting the critical roles of stereodefects and hydrogen-bonding interactions in promoting surface wetting and strengthening interfacial interactions.

The monomer sequence along the polymer backbone plays a critical role in determining material properties. Accordingly, the effects of stereodefect and hydrogen-bond distributions on thermomechanical and adhesive behavior were systematically investigated. With ~5 mol% of stereodefects and hydroxyl group introduced, *r*-PVL(OH)$_{4.9}$, *t*-PVL(OH)$_{5.0}$, and *m*-PVL(OH)$_{5.3}$ display similar melting transition behavior (Figure 5A, T_m = 47 to 49 °C) and comparable powder X-ray diffraction (XRD) profiles showing two characteristic peaks with 2θ values of 21.6° and 24.0° (Figure S28). These XRD peaks are attributed to the (110) and (200) planes of an orthorhombic crystal lattice, and their identical position and full width at half maximum (FWHM) value indicate that the crystal lattice remains largely unaffected by the distribution patterns of stereodefects and hydrogen-bonding groups. Despite similar crystal structures, *m*-PVL(OH)$_{5.3}$ exhibits the lowest degree of crystallinity (X_c = 26%) relative to *r*-PVL(OH)$_{4.9}$ (28%) and *t*-PVL(OH)$_{5.0}$ (31%) (Figure S29), resulting in the lowest modulus of 176 MPa (Tables S4-S6), which could benefit its adhesion performance. All three polymers display excellent mechanical performance, with extensibility approaching 1000% and tensile strength exceeding 14 MPa (Figure 5B). Among them, *m*-

PVL(OH)$_{5.3}$ achieves the highest toughness of 121 MJ m^{-3}, approximately 15% higher than *r*-PVL(OH)$_{4.9}$ (105 MJ m^{-3}) and *t*-PVL(OH)$_{5.0}$ (106 MJ m^{-3}). In addition, *m*-PVL(OH)$_{5.3}$ exhibits a lower water contact angle (82.1°) relative to *t*-PVL(OH)$_{5.0}$ (85.4°, Figure S30), suggesting a higher surface energy and better wettability. The synergistic combination of low modulus, high toughness, and enhanced wettability enables *m*-PVL(OH)$_{5.3}$ to achieve the highest adhesion strength of 12.3 MPa on steel, representing a 62% improvement over *t*-PVL(OH)$_{5.0}$ (Figure 5C). This result highlights the critical influence of monomer sequence on adhesion performance, likely arising from improved surface wetting and more effective energy dissipation. Remarkably, the adhesion performance of *m*-PVL(OH)$_{5.3}$ largely outperforms widely used UHU all-purpose glue and EVA hot melt, and is even superior to cyanoacrylate and polyurethane structural adhesives (Figure 5D). Furthermore, *m*-PVL(OH)$_{5.3}$ demonstrates strong and versatile adhesion (6.5–10.3 MPa) across a range of substrates, including iron, glass, poly(methyl methacrylate), wood, and bamboo (Figure 5E), underscoring its broad applicability in diverse practical scenarios.

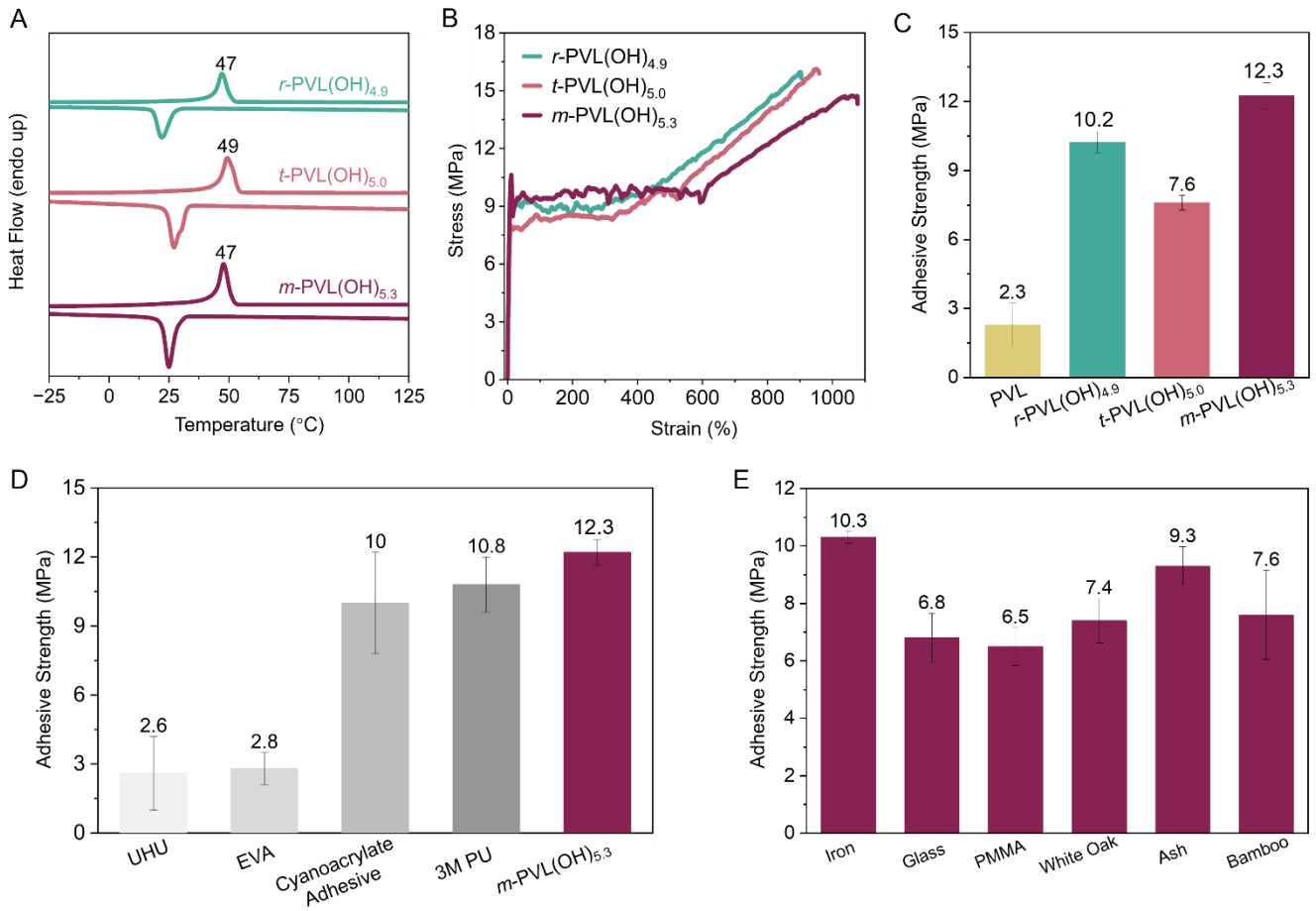


Figure 5. (A) DSC traces, (B) stress-strain curves, and (C) adhesion performance of *r*-PVL(OH)$_{4.9}$, *t*-PVL(OH)$_{5.0}$, and *m*-PVL(OH)$_{5.3}$. (D) Adhesion strength of common commercial glues and *m*-PVL(OH)$_{5.3}$ measured on stainless steel substrates. (E) Adhesion strength of *m*-PVL(OH)$_{5.3}$ on various substrates. Error bars represent a standard deviation of three specimens.

From an end-of-life perspective, particularly under natural conditions, biodegradability is a key attribute in the design of sustainable adhesives. However, in applications where materials can be efficiently collected at scale, chemical recycling of discarded materials into valuable monomers represents a complementary strategy for conserving chemical resources. Accordingly, the chemical recyclability of the developed polymers was systematically investigated. To establish baseline conditions, depolymerization of PVL was first examined under a reactive distillation set-up using reported catalysts, including $ZnCl_2$ and $Zn(Oct)_2$. Among these, $Zn(Oct)_2$ exhibited superior performance under identical conditions, affording a monomer yield of 87% (Table S7). Under optimized depolymerization conditions with a temperature of 140 °C and $Zn(Oct)_2$ loading of 6 wt% (Figures 6A and 6B), we achieved a high monomer recovery yield of 92% from *r*-$PVL(OH)_{4.9}$ (Table S7), which is in high purity as confirmed by its ^1H NMR spectrum (Figure 6C). Notably, the hydroxyl-substituted six-membered lactone was not recovered likely due to its much higher boiling temperature relative to δ-VL. This study demonstrates that the incorporation of hydroxyl side chains into PVL does not compromise its chemical recyclability, thereby providing the resulting adhesives with an additional sustainable end-of-life pathway alongside biodegradability.

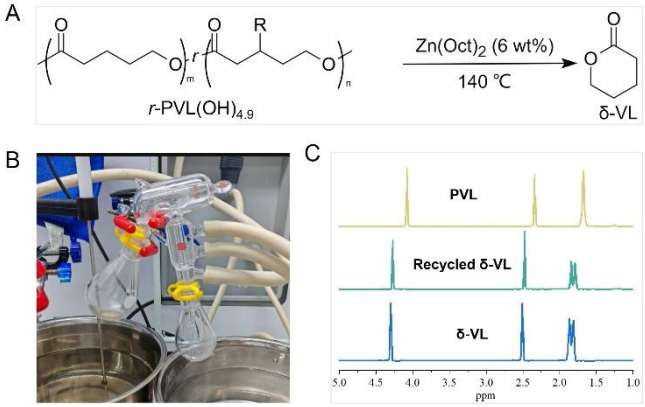


Figure 6. (A) The depolymerization route of *r*-$PVL(OH)_{4.9}$. (B) The reactive distillation set-up for the depolymerization investigation. (C) ^1H NMR overlay of PVL, recycled δ-VL, and pristine δ-VL.

Conclusion

In summary, we present a rational strategy for transforming biodegradable polyesters into strong and versatile adhesives. This approach is realized through the incorporation of stereodefects into the polymer backbone, the introduction of hydrogen-bonding interactions into side chains, and precise control over segment sequence through tailored copolymerization. Such structural engineering enables systematic tuning of surface wettability, crystalline morphology, thermomechanical properties, and viscoelastic behavior of the materials. The resulting PVL-based adhesives exhibit high mechanical toughness (>100 MJ m^{-3}), arising from optimized crystalline-domain morphology and enhanced cohesive interactions, as well as excellent adhesion strength (>10 MPa), enabled by improved interfacial wetting, efficient energy dissipation, and effective stress redistribution. This level of performance places the present system among the few sustainable adhesives that reach high-performance regime. Importantly, these bio-derived adhesives are biodegradable and chemically recyclable under mild conditions, offering dual end-of-life pathways. The strategy demonstrated herein sheds light on structure-regulated adhesive behavior in polyester systems and is expected to guide the development of other high-performance sustainable adhesives.

Methods

Materials and General Methods

All manipulations containing air- and/or moisture sensitive compounds were carried out under N_2 atmosphere or using glovebox techniques. Glassware was dried in a 120 °C oven for 1 h prior to use. Benzyl alcohol (BnOH, Energy Chemical Co.) was distilled prior to use. 1,4-Benzenedimethanol (BDM, Energy Chemical Co.) and 1,5,7-Triazabicyclo[4.4.0]dec-5-ene (TBD, Energy Chemical Co.) were sublimed prior to use. Deuterated chloroform ($CDCl_3$, Energy Chemical Co.), tri[N, N-bis(trimethylsilyl)amide]lanthanum ($La[N(SiMe_3)_2]_3$, Aladdin), 5,6-Dihydro-2H-Pyran-2-One (DPO, Energy Chemical Co.), triethylamine (Et_3N, Energy Chemical Co.), 2-Mercaptoethanol (β-ME, Energy Chemical Co.), Acetonitrile (ACN, Energy Chemical Co.), *tert*-butyldimethylsilyl chloride (TBSCl, Energy Chemical Co.), imidazole (Im, Energy Chemical Co.), propane-1-thiol (Energy Chemical Co.), triethylamine trihydrofluoride ($Et_3N{\cdot}3HF$, Energy Chemical Co.), Zinc chloride ($ZnCl_2$, Energy Chemical Co.), Zinc octoate

($Zn(Oct)_2$, Energy Chemical Co.) were used as received. The purchased δ-valerolactone (Energy Chemical Co.) and synthesized monomers were dried with CaH_2 and distilled or filtered before the polymerization studies.

Characterization

Wide-Angle X-Ray Diffraction Measurements: wide-angle X-Ray diffraction (WAXD) data were collected using a Rigaku SmartLab X-ray diffractometer equipped with a Cu-K_α X-ray source. The measurements were performed at a scan rate of 10°/min over a 2θ range from 10° to 60°.

Molar Mass Measurements: measurements of polymer weight-average molar mass (M_w), polymer number-average molar mass (M_n) and dispersity ($Đ = M_w/M_n$) were performed via size exclusion chromatography (SEC). The instrument is Agilent Infinity Lab LC Series with 1260 Infinity II Quaternary System and the analysis was performed at 25 °C with THF as the eluent at a flow rate of 0.5 mL/min.

NMR measurement: nuclear magnetic resonance (NMR) spectra were recorded on a JEOL JNM-ECZL500R or a Bruker AscendTM 400 spectrometer at ambient temperature (298 K). Chemical shifts for ^1H and DOSY spectra were referenced to the internal solvent resonances and reported as parts per million (ppm) relative to $CHCl_3$.

Thermal gravimetric analysis: on a Mettler Toledo TGA/DSC 3+ STARe System, TA Instrument was used to determine the decomposition temperature of polymers. Samples were heated from ambient temperature to 600 °C at a rate of 10 °C/min.

Differential scanning calorimetry (DSC): DSC measurements were performed using a DSC 2500 (Mettler Toledo DSC 3) at a heating rate of 10 °C/min. To eliminate thermal history, the 1st cooling and the 2nd heating curves were taken for plots.

Polarized Light Optical Microscopy (PLOM): polarized light optical microscope, Nikon ECLIPSE LV100N (Nikon, Tokyo, Japan), was used to obtain the PLOM images shown in Figure 3G of the main text. Films with ~50 μm thickness were prepared between two glass slides by heating the sample to 5 °C higher than the melting

temperature and keeping it at this temperature for 5 mins. Afterwards, the sample was cooled to 25 °C at 5 °C/min, and the images were taken after 24 h at 25 °C.

Dynamic mechanical analysis (DMA): DMA was carried out using a TA Instruments DMA 850 (Waters Corporation) equipped with a film tension clamp. Test specimens were cut from the same compression-molded films as those prepared for tensile testing, with typical dimensions of approximately 16.6 mm × 4 mm × 0.46 mm (length × width × thickness). Measurements were conducted under oscillatory deformation at a fixed frequency of 0.1 Hz. Temperature sweep experiments were carried out from 0 to 40 °C at a heating rate of 2 °C/min. The storage modulus (E'), loss modulus (E''), and loss tangent (tan δ) were recorded as a function of temperature using TA Instruments TRIOS software.

Rheological Analysis: rheological measurements were performed using an ARES-G2 rotational rheometer (TA Instruments) equipped with parallel circular plate geometry (25 mm diameter). Oscillatory frequency sweep tests were conducted over an angular frequency range of 0.1–100 rad/s at a constant temperature of 65 °C. A normal force of 0.05 N was applied to ensure proper contact between the sample and the plates. The strain amplitude was maintained within the linear viscoelastic region, as determined by preliminary strain sweep tests.

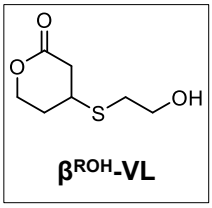
Mechanical Analysis: tensile stress-strain measurements were carried out using an Instron 68TM-30 universal testing system equipped with a 5 kN load cell. Dog-bone-shaped specimens (ASTM D638, Type V) were prepared via compression molding. Polymer samples were placed between non-stick Teflon sheets and pressed in a stainless-steel mold (45 × 60 × 0.4 mm). The molding process was conducted using a laboratory hot press with electrically heated platens at a temperature corresponding to the melting temperature (T_m) of each material. The molded sheets were subsequently cut into standard dog-bone specimens using an ASTM D638 Type V cutting die. The thickness (0.46 ± 0.01 mm), width (4.00 mm), and gauge length (16.6 ± 0.2 mm) of each specimen were measured and used for normalization by the Bluehill software (Instron). Prior to testing, specimens were mounted in a screw-tight grip fixture. Tensile tests were performed at ambient conditions with a crosshead speed of 5.0

mm/min until failure. Reported mechanical properties represent the average values obtained from multiple specimens for each sample.

Lap-Shear Measurement: samples for lap-shear testing were prepared according to a modified ASTM D1002 protocol. The polymer sample was placed between two substrates in a single-lap shear configuration with an overlapping area of approximately 20 mm × 5 mm, followed by heating with a heat gun to melt the polymer. Upon cooling to room temperature, the adhesive solidified and formed an interfacial bond between the adhesive layer and the substrates. The specimens were secured using binder clips and stored in a vacuum oven at 25 °C for 24 h prior to testing. Lap-shear measurements were conducted using an Instron 68TM-30 universal testing system equipped with a 5 kN load cell. The samples were mounted in screw-tight grips and tested at a crosshead speed of 5.0 mm/min under ambient conditions. The adhesive strength (MPa) was calculated by dividing the maximum force (N) recorded during the test by the bonded area (mm²) of the adhesive.

General synthesis Procedures.

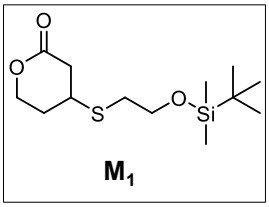
Synthesis of β^{ROH}-VL



β^{ROH}-VL

5,6-dihydro-2H-pyran-2-one (9.90 g, 0.1 mol) dissolved in 238 mL of acetonitrile was added to a 500 mL flask. After adding 2-mercaptoethanol (7.89 g, 0.1 mol), the mixture was thoroughly stirred, followed by the addition of triethylamine (10.22 g, 0.1 mol) under an ice water bath. After 5 mins, the ice water bath was removed and the reaction mixture was kept stirring at rt for 2 h. After the reaction is complete, the product was obtained by removing the solvent through rotary evaporation (17 g, ~90% yield). ^{1}H NMR (500 MHz, $CDCl_3$): δ 4.48 (m,1H, -C*H*$_2$OOC-), 4.25 (m, 1H, - C*H*$_2$OOC -), 3.73 (t, 2H, -C*H*$_2$O-), 3.28 (m, 1H, -C*H*-), 2.94 (m, 1H, -CH$_2$OOCC*H*$_2$-), 2.73 (t, 2H, -SC*H*$_2$-), 2.54-2.46 (m, 1H, -CH$_2$OOCC*H*$_2$-), 2.21 (m, 1H, -CHC*H*$_2$CH$_2$-), 1.89-1.79 (m, 1H, -CHC*H*$_2$CH$_2$-).

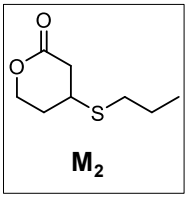
Synthesis of M_1



M_1

To a stirred solution of β^{ROH}-VL (18.00 g, 0.1 mol) in THF (200 mL) was added imidazole (10.33 g, 0.15 mol) and *tert*-butyldimethylsilyl chloride (19.81 g, 0.13 mol) at rt. After 2 h, H_2O (200 mL) was added, and the mixture was diluted with DCM (200 mL). The layers were separated, and the aqueous layer was extracted with DCM (3×200 mL). The combined organic layers were washed with brine (500 mL), dried with anhydrous Na_2SO_4, and evaporated. The residue was purified by flash chromatography (petroleum ether) to give the pale-yellow oil compound (22 g) in ~79.3% yield. ^{1}H NMR (500 MHz, $CDCl_3$): δ 4.46 (m, 1H, -C*H*$_2$OOC-), 4.26-4.18 (m, 1H, -C*H*$_2$OOC-), 3.75 (t, 2H, -SCH$_2$C*H*$_2$O-), 3.31 (m, 1H, -C*H*-), 2.92 (m, 1H, -CH$_2$OOCC*H*$_2$-), 2.65 (t, 2H, -SC*H*$_2$-), 2.47 (m, 1H, -CH$_2$OOCC*H*$_2$-), 2.18 (m, 1H, -CHC*H*$_2$CH$_2$-), 1.82 (m, 1H, -CHC*H*$_2$CH$_2$-), 0.84 (s, 9H, -CC*H*$_3$-), 0.02 (s, 6H, -C*H*$_3$).

Synthesis of M_2



M_2

The synthetic procedure of M_2 is the same with that of β^{ROH}-VL except that 2-mercaptoethanol was replaced with propane-1-thiol. ^{1}H NMR (500 MHz, $CDCl_3$): δ 4.39 (m, 1H, -C*H*$_2$OOC-), 4.18 (m, 1H, -C*H*$_2$OOC-), 3.12 (m, 1H, -C*H*-), 2.82 (m, 1H, -CH$_2$OOCC*H*$_2$-), 2.43 (t, 2H, -SC*H*$_2$-), 2.38 (m, 1H, -CH$_2$OOCC*H*$_2$-), 2.11 (m, 1H, -CHC*H*$_2$CH$_2$-), 1.74 (m, 1H, -CHC*H*$_2$CH$_2$-), 1.50 (m, 2H, -C*H*$_2$CH$_3$), 0.88 (t, 3H, -C*H*$_3$).

Synthesis of *r*-PVL(OH)$_X$: In a glove box, a 1 mol/L toluene solution of BnOH was prepared and mixed with La[N(SiMe$_3$)$_2$]$_3$ solution (1 mol/L in toluene) in a pre-determined ratio. The mixture was stirred at rt for 5–10 min in a 2 mL vial. In a 20 mL vial containing a stir bar, M_1, and *δ*-VL, the mixed solution of initiator and catalyst was added to initiate the polymerization. After 1 h, the polymerization was quenched by DCM solution of benzoic acid (10 mg/mL). Triethylamine trihydrofluoride was added to the mixture, followed by stirring overnight to achieve the deprotection of hydroxyl groups. The mixture was precipitated into cold methanol, filtered, and collected. After two

more precipitation cycles, the polymer was collected and dried in a vacuum oven at 45 °C overnight to a constant weight.

Synthesis of *t*-PVL(OH)$_X$: In a glove box, a 1 mol/L THF solution of 1,4-Benzenedimethanol (BDM) was mixed with La[N(SiMe$_3$)$_2$]$_3$ solution (1 mol/L in toluene) in a pre-determined ratio. The mixture was stirred at rt for 5–10 min in a 2 mL vial. In a 20 mL vial containing a stir bar and δ-VL, the mixed solution of initiator and catalyst was added to initiate the polymerization. After the reaction completed, M$_1$ was added to the vial, and the reaction was allowed to proceed for another 2–3 h. The polymerization was then quenched by DCM solution of benzoic acid (10 mg/mL). Triethylamine trihydrofluoride was added to the mixture, followed by stirring overnight to achieve deprotection of the hydroxyl groups. The mixture was precipitated into cold methanol, filtered, and collected. After two more precipitation cycles, the polymer was collected and dried in a vacuum oven at 45 °C overnight to a constant weight.

Synthesis of *m*-PVL(OH)$_X$: In a glove box, a 1 mol/L THF solution of 1,4-Benzenedimethanol (BDM) was mixed with La[N(SiMe$_3$)$_2$]$_3$ solution (1 mol/L in toluene) in a pre-determined ratio. The mixture was stirred at rt for 5–10 min in a 2 mL vial. In a 20 mL vial containing a stir bar, *δ*-VL and M1 (3:1), the mixed solution of initiator and catalyst was added to initiate the polymerization. After the reaction completed, *δ*-VL was added to the vial, and the reaction was allowed to proceed for another 2–3 h. The polymerization was quenched by DCM solution of benzoic acid (10 mg/mL). Triethylamine trihydrofluoride was added to the system, followed by stirring overnight to achieve deprotection of the hydroxyl groups. The mixture was precipitated into cold methanol, filtered, and collected. After two more precipitation cycles, the polymer was collected and dried in a vacuum oven at 45 °C overnight to a constant weight.

Synthesis of *r*-PVL(3C)$_X$: In a glove box, a 1 mol/L toluene solution of BnOH was mixed with La[N(SiMe$_3$)$_2$]$_3$ solution (1 mol/L in toluene) in a pre-determined ratio. The mixture was stirred at rt for 5–10 mins. In a 20 mL vial containing a stir bar, M$_2$, and *δ*-VL, the mixed solution of initiator and catalyst were added to initiate the

polymerization. After 2 h, the polymerization was quenched by DCM solution of benzoic acid (10mg/mL). The mixture was precipitated into cold methanol, filtered, and collected. After two more precipitation cycles, the polymer was collected and dried in a vacuum oven at 45 °C overnight to a constant weight.

Acknowledgements

We gratefully acknowledge support by the National Natural Science Foundation of China (22501089, Z.Z.; 22473044, Y. C.) and Fundamental Research Funds for the Central Universities (grant no. 2025ZYGXZR079, Z.Z.).

Author contributions

Conceptualization: Z. Zhang. Methodology: Z. Zhang and B. Mo. Investigation: B. Mo, L. Zhu, Z. Xiao, and B. Wang. PLOM: B. Mo and Y. Cao. Funding acquisition: Z. Zhang and Y. Cao. Writing-original draft: B. Mo and L. Zhu. Writing-review & editing: All authors.

References

[1]. Dinte, E.; Sylvester, B., Adhesives: applications and recent advances. *Applied adhesive bonding in science and technology* **2018**, 119-134.

[2]. Brockmann, W.; Geiß, P. L.; Klingen, J.; Schröder, K. B., *Adhesive bonding: materials, applications and technology*. John Wiley & Sons: 2009.

[3]. Heinzmann, C.; Weder, C.; de Espinosa, L. M., Supramolecular polymer adhesives: advanced materials inspired by nature. *Chem. Soc. Rev.* **2016,** *45* (2), 342-358.

[4]. Nam, S.; Mooney, D., Polymeric tissue adhesives. *Chem. Rev.* **2021,** *121* (18), 11336-11384.

[5]. Eisen, A.; Bussa, M.; Röder, H., A review of environmental assessments of biobased against petrochemical adhesives. *J. Clean. Prod.* **2020,** *277*, 124277.

[6]. Packham, D., The environmental impact of adhesives. In *Eco-efficient Construction and Building Materials*, Elsevier: 2014; pp 338-367.

[7]. Sands, J. M.; Fink, B. K.; McKnight, S. H.; Newton, C. H.; Gillespie Jr, J. W.; Palmese, G. R., Environmental issues for polymer matrix composites and structural adhesives. *Clean Prod. Processes* **2001,** *2* (4), 228-235.

[8]. Gierenz, G.; Karmann, W., *Adhesives and adhesive tapes*. John Wiley & Sons: 2008.

[9]. Zhu, Y.; Romain, C.; Williams, C. K., Sustainable polymers from renewable resources. *Nature* **2016,** *540* (7633), 354-362.

[10]. Korley, L. T.; McNeil, A. J.; Coates, G. W., Challenges and opportunities in sustainable polymers. ACS Publications: 2022; Vol. 55, pp 2543-2544.

[11]. Cywar, R. M.; Rorrer, N. A.; Hoyt, C. B.; Beckham, G. T.; Chen, E. Y.-X., Bio-based polymers with performance-advantaged properties. *Nat. Rev. Mater.* **2022,** *7* (2), 83-103.

[12]. Huang, H.-Y.; Xiong, W.; Huang, Y.-T.; Li, K.; Cai, Z.; Zhu, J.-B., Spiro-salen catalysts enable the chemical synthesis of stereoregular polyhydroxyalkanoates. *Nat. Catal.* **2023,** *6* (8), 720-728.

[13]. Zhang, Z.-H.; Sun, Y.; Rajeshkumar, T.; Li, Y.; Maron, L.; Hong, M., Vinyl polymers with fully degradable carbon backbones enabled by aromatization-driven C–C bond cleavage. *Nat. Chem.* **2025,** *17* (5), 746-755.

[14]. Radano, C. P.; Baker, G. L.; Smith, M. R., Stereoselective polymerization of a racemic monomer with a racemic catalyst: direct preparation of the polylactic acid stereocomplex from racemic lactide. *Journal of the American Chemical Society* **2000,** *122* (7), 1552-1553.

[15]. Quinn, E. C.; Westlie, A. H.; Sangroniz, A.; Caputo, M. R.; Xu, S.; Zhang, Z.; Urgun-Demirtas, M.; Muller, A. J.; Chen, E. Y.-X., Installing controlled stereo-defects yields semicrystalline and biodegradable poly (3-hydroxybutyrate) with high toughness and optical clarity. *J. Am. Chem. Soc.* **2023,** *145* (10), 5795-5802.

[16]. Zhang, Z.; Quinn, E. C.; Kenny, J. K.; Grigoropoulos, A.; DesVeaux, J. S.; Chen, T.; Zhou, L.; Xu, T.; Beckham, G. T.; Chen, E. Y.-X., Stereomicrostructure-regulated biodegradable adhesives. *Science* **2025,** *387* (6731), 297-303.

[17]. Pal, S.; Shin, J.; DeFrates, K.; Arslan, M.; Dale, K.; Chen, H.; Ramirez, D.; Messersmith, P. B., Recyclable surgical, consumer, and industrial adhesives of poly (α-lipoic acid). *Science* **2024,** *385* (6711), 877-883.

[18]. Rahman, M. A.; Bowland, C.; Ge, S.; Acharya, S. R.; Kim, S.; Cooper, V. R.; Chen, X. C.; Irle, S.; Sokolov, A. P.; Savara, A., Design of tough adhesive from commodity thermoplastics through dynamic crosslinking. *Sci. Adv.* **2021,** *7* (42), eabk2451.

[19]. Westerman, C. R.; McGill, B. C.; Wilker, J. J., Sustainably sourced components to generate high-strength adhesives. *Nature* **2023,** *621* (7978), 306-311.

[20]. Yang, G.; Gong, Z.; Luo, X.; Chen, L.; Shuai, L., Bonding wood with uncondensed lignins as adhesives. *Nature* **2023,** *621* (7979), 511-515.

[21]. McKee, J. R.; Huokuna, J.; Martikainen, L.; Karesoja, M.; Nykänen, A.; Kontturi, E.; Tenhu, H.; Ruokolainen, J.; Ikkala, O., Molecular engineering of fracture energy dissipating sacrificial bonds into cellulose nanocrystal nanocomposites. *Angew. Chem. Int. Ed.* **2014,** *126* (20), 5149-5153.

[22]. Shi, Q.; Zhang, Z.; Liu, S., Precision Sequence-Defined Polymers: From Sequencing to Biological Functions. *Angew. Chem. Int. Ed.* **2024,** *136* (6), e202313370.

[23]. Lutz, J.-F.; Ouchi, M.; Liu, D. R.; Sawamoto, M., Sequence-controlled polymers. *Science* **2013,** *341* (6146), 1238149.

[24]. Badi, N.; Lutz, J.-F., Sequence control in polymer synthesis. *Chem. Soc. Rev.* **2009,** *38* (12), 3383-3390.

[25]. Qin, J.; Dou, Y.; Wen, J.; Tang, X., Facilely Accessible and Reusable High-Performance Poly (Thioester Amide) Adhesives with Exceptional Versatility and Environmental Stability. *Adv. Mater.* **2026,** *38* (4), e06748.

[26]. Zhao, Y.; Rettner, E. M.; Harry, K. L.; Hu, Z.; Miscall, J.; Rorrer, N. A.; Miyake, G. M., Chemically recyclable polyolefin-like multiblock polymers. *Science* **2023,** *382* (6668), 310-314.

[27]. Weng, C.; Li, X.; Tang, X., Solvent-Dependent Sequence-Controlled Copolymerization of Lactones: Tailoring Material Properties from Robust Plastics to Tough Elastomers. *Angew. Chem. Int. Ed.* **2025,** *64* (3), e202415388.

[28]. Li, C.; Wang, L.; Yan, Q.; Liu, F.; Shen, Y.; Li, Z., Rapid and controlled polymerization of bio-sourced δ-caprolactone toward fully recyclable polyesters and thermoplastic elastomers. *Angew. Chem. Int. Ed.* **2022,** *134* (16), e202201407.

[29]. Hu, Z.; Wolff, A. M.; Zhao, Y.; Rettner, E. M.; Alam, M. S.; Frederick, T.; Sangroniz, A.; Miyake, G. M., Sustainable Structural Hot-Melt Adhesives Enabled by Functionalized Crystalline Lamellae. *Adv. Mater.* **2026,** *38* (8), e18259.

[30]. Tournier, V.; Duquesne, S.; Guillamot, F.; Cramail, H.; Taton, D.; Marty, A.; André, I., Enzymes' power for plastics degradation. *Chem. Rev.* **2023,** *123* (9), 5612-5701.

[31]. Lee, H.; Zeng, F.; Dunne, M.; Allen, C., Methoxy poly (ethylene glycol)-block-poly (δ-valerolactone) copolymer micelles for formulation of hydrophobic drugs. *Biomacromolecules* **2005,** *6* (6), 3119-3128.

[32]. Mishra, G. P.; Kinser, R.; Wierzbicki, I. H.; Alany, R. G.; Alani, A. W., In situ gelling polyvalerolactone-based thermosensitive hydrogel for sustained drug delivery. *Eur. J. Pharm. Biopharm.* **2014,** *88* (2), 397-405.

[33]. Toncheva, V.; Van Den Bulcke, A.; Schacht, E.; Mergaert, J.; Swings, J., Synthesis and environmental degradation of polyesters based on poly (ε-caprolactone). *J. Environ. Polym. Degrad.* **1996,** *4* (2), 71-83.

[34]. Li, X. L.; Clarke, R. W.; An, H. Y.; Gowda, R. R.; Jiang, J. Y.; Xu, T. Q.; Chen, E. Y. X., Dual recycling of depolymerization catalyst and biodegradable polyester that markedly outperforms polyolefins. *Angew. Chem. Int. Ed.* **2023,** *135* (26), e202303791.

[35]. Han, C.-T.; Ma, K.; Zhang, Z.; Clarke, R. W.; Gowda, R. R.; Xu, T.-Q.; Chen, E. Y.-X., Circular polymer designed by regulating entropy: spiro-valerolactone-based polyesters with high gas barriers and adhesion strength. *J. Am. Chem. Soc.* **2025,** *147* (5), 4511-4519.

[36]. Zhang, J.; Hu, W., Roles of specific hydrogen-bonding interactions in the crystallization kinetics of polymers. *Polymer* **2023,** *283*, 126278.

[37]. Wan, Q.; Thompson, B. C., Control of properties through hydrogen bonding interactions in conjugated polymers. *Adv. Sci.* **2024,** *11* (8), 2305356.

[38]. Song, P. a.; Xu, Z.; Guo, Q., Bioinspired strategy to reinforce PVA with improved toughness and thermal properties via hydrogen-bond self-assembly. *ACS Macro Lett.* **2013,** *2* (12), 1100-1104.

[39]. Valiokas, R.; Östblom, M.; Svedhem, S.; Svensson, S. C.; Liedberg, B., Thermal stability of self-assembled monolayers: Influence of lateral hydrogen bonding. *J. Phys. Chem. B.* **2002,** *106* (40), 10401-10409.

[40]. Song, P.; Wang, H., High-performance polymeric materials through hydrogen-bond cross-linking. *Adv. Mater.* **2020,** *32* (18), 1901244.

[41]. Lebedev, A. A. Y. B. V. L. T. G. K. N. K., The calorimetric study in the 13·8–340°K range of δ-valerolactone, its polymer, and of the δ-valerolactone polymerization. *Polym. Sci. U.S.S.R.* **1982,** *24* (24), 9.

[42]. Ma, B.; Yang, Y.; Wang, J.; Yu, Z.; Wu, P., Harnessing Water Molecules for Strong Underwater Adhesion. *Adv. Mater.* **2026**, e73571.

[43]. Mazzotta, M. G.; Putnam, A. A.; North, M. A.; Wilker, J. J., Weak bonds in a biomimetic adhesive enhance toughness and performance. *J. Am. Chem. Soc.* **2020,** *142* (10), 4762-4768.

Supplementary Files

This is a list of supplementary files associated with this preprint. Click to download.

- PVLOHAdhesivesSI.docx